HHS Public Access

Author manuscript

Eur J Nucl Med Mol Imaging. Author manuscript; available in PMC 2016 November 01.

Published in final edited form as:

Eur J Nucl Med Mol Imaging. 2015 November ; 42(12): 1859–1868. doi:10.1007/s00259-015-3085-7.

Evaluation of Two Novel ^{64}Cu-labelled RGD Peptide Radiotracers for Enhanced PET Imaging of Tumor Integrin $\alpha_v\beta_3$

Reinier Hernandez[1], **Andrzej Czerwinski**[2], **Rubel Chakravarty**[3], **Yunan Yang**[3], **Christopher G. England**[1], **Stephen A. Graves**[1], **Robert J. Nickles**[1], **Francisco Valenzuela**[2], and **Weibo Cai**[1,3,4]

[1]Department of Medical Physics, University of Wisconsin - Madison, WI, USA, 53705

[2]Peptides International, Inc., Louisville, K Y, USA, 40299

[3]Department of Radiology, University of Wisconsin - Madison, WI, USA, 53705

[4]University of Wisconsin Carbone Cancer Center, Madison, WI, USA, 53705

Abstract

Purpose—Our goal was to demonstrate that suitably derivatized monomeric RGD peptide-based PET tracers, targeting integrin $\alpha_v\beta_3$, may offer advantages in image contrast, time for imaging, and low uptake in non-target tissues.

Methods—Two cyclic RGDfK derivatives, $(PEG)_2$-c(RGDfK) and PEG_4-SAA_4-c(RGDfK), were constructed and conjugated to NOTA for ^{64}Cu labeling. Their integrin $\alpha_v\beta_3$-binding properties were determined via a competitive cell binding assay. Mice bearing U87MG tumors were intravenously injected with each of the ^{64}Cu-labelled peptides, and PET scans were acquired during the first 30 min, and 2 and 4 h post-injection (p.i.). Blocking and *ex vivo* biodistribution studies were carried out to validate the PET data and confirm the specificity of the tracers.

Results—The IC_{50} values of NOTA-$(PEG)_2$-c(RGDfK) and NOTA-PEG_4-SAA_4-c(RGDfK) were 444 ± 41, and 288 ± 66 nM, respectively. Dynamic PET data of ^{64}Cu-NOTA-$(PEG)_2$-c(RGDfK) and ^{64}Cu-NOTA-PEG_4-SAA_4-c(RGDfK) unveiled similar circulation $t_{1/2}$ and peak tumor uptake of ~4 %ID/g for both tracers. Due to its marked hydrophilicity, ^{64}Cu-NOTA-PEG_4-SAA_4-c(RGDfK) provided faster clearance from tumor and normal tissues yet maintaining excellent tumor-to-background ratios. Static PET scans at later time-points corroborated the enhanced excretion of the tracer, especially from abdominal organs. *Ex vivo* biodistribution and receptor blocking studies confirmed the accuracy of the PET data and the integrin $\alpha_v\beta_3$-specificity of the peptides.

Corresponding author: Weibo Cai, PhD, wcai@uwhealth.org; phone: 608-262-1749;f ax: 608-265-0614.

Conflict of Interest: Andrzej Czerwinski and Francisco Valenzuela are employees of Peptides International, Inc. The other authors declared that they have no conflict of interest.

Ethical Approval: All procedures performed in studies involving animals were in accordance with the ethical standards of the University of Wisconsin Institutional Animal Care and Use Committee.

Compliance with Ethical Standards

This article does not contain any studies with human participants performed by any of the authors.

Conclusion—Our two novel RGD-based radiotracers with optimized pharmacokinetic properties allowed a fast, high-contrast PET imaging of tumor associated integrin $\alpha_v\beta_3$. These tracers may facilitate the imaging of abdominal malignancies, normally precluded by high background uptakes.

Keywords

Integrin $\alpha_v\beta_3$; Copper-64 (^{64}Cu); RGD peptide; angiogenesis; positron emission tomography (PET); molecular imaging

Introduction

The expression of several integrins is essential for the induction and sustainment of tumor angiogenesis [1, 2]. Particularly, integrin $\alpha_v\beta_3$ is closely associated with aggressiveness and a poor prognosis in several malignancies including breast cancer, ovarian cancer, melanoma, and glioblastoma [2–5]. Integrin $\alpha_v\beta_3$ is a membrane protein that strongly binds to extracellular matrix (ECM) proteins (*e.g.* fibronectin and vimentin) through its interaction with arginine-glycine-aspartic acid (RGD) tripeptides. Over the last two decades, peptides containing the RGD motif have been widely employed for the imaging and targeted therapy of tumors overexpressing integrin $\alpha_v\beta_3$ [6–11]. The body of work on tumor targeting using RGD peptides is extensive, being the radiolabeling of such vectors for noninvasive positron emission tomography (PET) and single photon emission tomography (SPECT) imaging of the *in vivo* integrin $\alpha_v\beta_3$ expression predominant.

The success attained using these radiotracers have led to several human trials employing ^{18}F radiolabeled RGD peptides for PET imaging [12, 13]. However, the clinical implementation of these agents has been halted by several difficulties including their synthesis and unfavorable pharmacokinetic (PK) profiles. In an effort to improve the overall tumor uptake of these tracers, several strategies have been adopted including the cyclization of the peptides -to enhance enzymatic instability- and/or the synthesis of multimeric RGD analogs that show improved tumor accumulation/retention. The latter enhancement on tumor accretion has been credited to the binding of the multimeric peptide to more than one target, or more plausibly, to a statistical effect given the increased local concentration of RGD moieties. However, such improvement comes at the expense of increasing off-target uptakes of the tracer on significant organs such as liver, spleen, intestines, and muscle, which negatively impacts image contrast and increment procedural doses.

In this work, we sought to synthesize and evaluate two structurally modified RGD peptides with enhanced PK properties that allow excellent tumor targeting, while keeping off-target uptakes at negligible levels. The peptides featured a monomeric cyclic RGDfK motif with a combination of 8-amino-3,6-dioxaoctanoic acid (PEG), 15-amino-4,7,10,13-tetraoxapentadecanoic acid (PEG_4), and/or 7-amino-L-glycero-Lgalacto-2,6-anhydro-7-deoxyheptanamide (SAA) linkers. Subsequently, we conjugated the modified peptides $(PEG)_2$-c(RGDfK) and PEG_4-SAA_4-c(RGDfK), to the chelator 1,4,7-triazacyclononane-triacetic acid (NOTA) for radiolabeling with ^{64}Cu. The acquisition of dynamic PET scan allowed us to evaluate and compare the *in vivo* PK and tumor targeting properties of NOTA-

c(RGDfK), NOTA-$(PEG)_2$-c(RGDfK), and NOTA-PEG_4-SAA_4-c(RGDfK), in athymic nude mice bearing integrin $\alpha_v\beta_3$-positive human glioblastoma (U87MG) tumors. Finally, competitive cell binding, receptor blocking, and biodistribution studies were also performed to confirm that integrin $\alpha_v\beta_3$ binding affinity and specificity of the modified peptides was conserved.

Materials and Methods

Reagents

All chemicals employed were of the highest purity available and used without further purification. The catalog peptides c(RGDfK) and $(PEG)_2$-c(RGDfK), along with the custom synthesis product PEG_4-SAA_4-c(RGDfK), were all supplied by Peptides International, Inc. (Louisville, KY). Chelex 100 resin (50–100 mesh) was obtained from Sigma-Aldrich (St. Louis, MO) and 2-(p-isothiocyanatobenzyl)-NOTA (p-SCN-Bn-NOTA) was purchased from Macrocyclics (Dallas, TX). When not indicated otherwise, materials and reagents were obtained from Thermo Fisher Scientific (Fair Law, NJ). Water and all buffers were of Milli-Q grade (resistivity > 18.2 MΩ·cm) and were treated with Chelex 100 resin to remove heavy metal contaminants.

NOTA conjugation and ^{64}Cu radiolabeling

The conjugation of NOTA was performed using a previously described method with slight modifications [14]. Briefly, in a 1.5 mL Eppendorf vial, 2 mg of each peptide (~3.3 nmol, ~2.2 nmol, and ~1.25 nmol of c(RGDfK), $(PEG)_2$-c(RGDfK) and PEG_4-SAA_4-c(RGDfK), respectively) were dissolved in phosphate buffer saline (PBS) and the pH adjusted to 9.0 with 0.1 M Na_2CO_3. Subsequently, a freshly prepared solution of p-SCN-Bn-NOTA in DMSO (~20 mg/mL) was added to the peptide solution for a peptide: p-SCN-Bn-NOTA ratio of 1:2, and the reaction was carried out for 2h at room temperature; the concentration of DMSO was kept below 5% v:v. The conjugated peptides were separated using semi-preparative HPLC (conditions: column, Phenomenex Luna C18, 5 μm, 10 × 250 mm; flow, 5 mL/min; mobile phase, 5–65% acetonitrile/water linear gradient in 40 min) and the product lyophilized to yield a white powder. MALDI-TOF-MS was performed to confirm the identity of the purified product.

For ^{64}Cu radiolabeling, 10 μL of a peptide stock solution (1 mg/mL) were reacted with 74 MBq (2 mCi) of $^{64}CuCl_2$ in 300 μL of NaOAc buffer (0.1 M, pH = 4.5) at 37 °C for 15 min, under constant shaking. The radiolabeled peptides were then separated by analytical HPLC (conditions: column, Acclaim 120 C18, 5μm, 4.6 × 250 mm; flow, 1 mL/min; mobile phase, 5–65% ethanol/water linear gradient in 40 min), the radioactive fractions collected, diluted in PBS for a final <10% EtOH concentration, and filtered through a 20 μm syringe filter. The radiochemical purity and labeling yields were estimated from the radio-chromatograms.

Octanol–water partition coefficient

Hydrophilicity of ^{64}Cu-NOTA-c(RGDfK), ^{64}Cu-NOTA-$(PEG)_2$-c(RGDfK), and ^{64}Cu-NOTA-PEG_4-SAA_4-c(RGDfK) was evaluated through an octanol-water distribution study. Fifteen μCi (~0.6 MBq) of the radiolabeled peptide of interest were added to 2 mL of 1:1 n-

octanol:water mixture. The mixture was vigorously mixed and allowed to reach equilibrium for 1 h. After reaching equilibrium, the mixture was centrifuged to separate the two phases (5 min; 5000 rpm). Lastly, the radioactivity in each phase was quantified in an automated γ-counter (Perkin Elmer) and logP values for each compound were determined in triplicate.

Cell lines and animal model

Human glioblastoma U87MG cells were obtained from the American Type Culture Collection (ATCC, Manassas, VA). Cells were cultured in Dulbecco's Modified Eagle's Medium (Invitrogen, Carlsbad, CA)supplemented with penicillin (100 U/mL), streptomycin (100 μg/mL), fetal bovine serum (10%, Sigma-Aldrich, St. Louis, MO) and incubated at 37°C in a 5% CO_2 atmosphere. Cells were used for *in vitro* experiments and tumor induction once ~80% confluence was reached. All animal studies were conducted under a protocol approved by the University of Wisconsin Institutional Animal Care and Use Committee. U87MG tumor xenografts were induced in 5-week-old female/male athymic nude mice (Harlan, Indianapolis, IN) by subcutaneous injection of 5×10^6 cells suspended in 100 μl of 1:1 mixture of DMEM culture medium and Matrigel (BD Biosciences, Franklin lakes, NJ), into the mice lower flank. Tumor size was visually inspected every other day and the animals were employed for *in vivo* imaging experiments when tumors reached 5–10 mm in diameter, ~3 weeks after cell implantation.

Competitive Cell Binding Assay

Following our previously reported method, the integrin $\alpha_v\beta_3$ specificity and binding affinity of NOTA-c(RGDfK), NOTA-$(PEG)_2$-c(RGDfK), and NOTA-PEG_4-SAA_4-c(RGDfK) were evaluated via a competitive binding assay using ^{125}I-echistatin (PerkinElmer, Waltham, MA) as the integrin-specific radio-ligand [15]. Briefly, 1×10^5 U87MG cells where seeded into 96-well filter plates (EMD Millipore Corp., Billerica, MA) and incubated with ^{125}I-Echistatin (~10,000 cpm) for 2 h at room temperature in the presence of increasing concentration of the RGD-based peptides. Subsequently, wells were washed with PBS to remove unbound activity, the plates were blow dried, and the PVDF filters were removed and counted in an automated γ-counter (PerkinElmer, Waltham, MA). Each data point was replicated three times, plotted in GraphPad Prism (GraphPad Software, San Diego, CA) and one-site binding curves were fitted to determine the 50% inhibition concentration (IC_{50}) values.

Small animal PET imaging

The acquisition of the PET images was performed in an Inveon microPET/microCT scanner (Siemens Preclinical Solutions, Knoxville, TN). For *in vivo* dynamic PET studies, two U87MG tumor bearing mice per group were anesthetized with isofluorane 2%, the tail vein catheterized, and placed in the scanner in a prone position. Simultaneously with the injection of 5.5 MBq (150 μCi) of either ^{64}Cu-NOTA-c(RGDfK), ^{64}Cu-NOTA-$(PEG)_2$-c(RGDfK), or ^{64}Cu-NOTA-PEG_4-SAA_4-c(RGDfK), a 30 min dynamic scan was performed and framed into 28 frames :5×6 sec, 7×30 sec, 6×60 sec, 6×120 sec, and 2×240 sec; the last frame was consider equivalent to a 30 min post injection (p.i.) static scan. An additional mouse was added to each group to complete n = 3, and longitudinal static scans were recorded at 30

min, 2 h, and 4 h p.i. In a fourth group (n = 4) corresponding to a receptor blocking experiment, U87MG bearing mice were co-administered with 5.5 MBq of ^{64}Cu-NOTA-PEG$_4$-SAA$_4$-c(RGDfK) and a blocking dose (10 mg/kg) of c(RGDyK), then sequential scans were performed at 30 min, 2 h, and 4 h after administration. Twenty million coincidence events per mouse were acquired for every static PET emission scan. Image reconstructions were performed on an Inveon Acquisition Workplace (Siemens Preclinical Solutions, Knoxville, TN) workstation using an ordered subset expectation maximization 3D/maximum a posteriori (OSEM3D/MAP) reconstruction algorithm. Tissue uptakes were quantified from a region-of-interest (ROI) analysis of the PET images and expressed as percentage of the injected dose per gram (%ID/g).

Biodistribution Studies

To confirm the accuracy of the quantitative PET data and obtain a detailed tissue distribution of the tracers, a biodistribution study was performed. Immediately after the last PET scan at 4 h p.i., mice were euthanized by CO_2 asphyxiation and blood, U87MG tumor, and other major organs collected and weighted. The radioactivity contained in each tissue was measured in an automated γ-counter (Perkin Elmer), and the %ID/g calculated and reported as mean ± SD.

Stability

Serum and metabolic stability of peptides was determined using radio-HPLC. For serum stability, radiolabeled peptides were incubated with reconstituted mouse serum at 37°C for 1 and 4 h. After incubation, equal amount of acetonitrile was added to the mixture to precipitate serum proteins. Samples were centrifuged at 5000 rpm for 5 min and the supernatant was collected, filtered through a 0.2 μm filter, and analyzed by HPLC. For metabolic studies, normal ICR mice were injected with ~300 μCi of tracer and placed under shallow anesthesia. After 1 h urine samples were collected, mixed with acetonitrile 1:1, centrifuged, and the supernatant collected, filtered, and analyzed by HPLC.

Statistical Analysis

To ensure the statistical power of the studies, all groups had a minimum of three subjects ($n \geq 3$). Quantitative data were presented as mean ± SD. Means were compared using two sample Student's t test; a $P < 0.05$ was considered statistically significant.

Results

Synthesis, radiolabeling, and characterization

The conjugates NOTA-c(RGDfK), NOTA-(PEG)$_2$-c(RGDfK), and NOTA-PEG$_4$-SAA$_4$-c(RGDfK) were synthesized via standard isothiocyanate chemistry and separated using semi-preparative reverse-phase HPLC. Fig. 1 shows the structure of the purified peptides which identity was confirmed by MALDI-TOF mass spectrometry (Online Resource Fig. S1) analysis: NOTA-c(RGDfK) ($[M+H]^+_{calc}$ = 1054.5 vs. $[M+H]^+_{det}$ = 1054.4), NOTA-(PEG)$_2$-c(RGDfK) ($[M+H]^+_{calc}$ = 1344.6 vs. $[M+H]^+_{det}$ = 1344.6), and NOTA-PEG$_4$-SAA$_4$-c(RGDfK) ($[M+H]^+_{calc}$ = 2057.9 vs. $[M+H]^+_{det}$ = 2057.8). Radiolabeling of the three peptides with ^{64}Cu was accomplished within 15 min at room temperature, and ^{64}Cu-NOTA-

c(RGDfK) (Rt = 20.4 min), ^{64}Cu-NOTA-$(PEG)_2$-c(RGDfK) (Rt = 20.7 min), and ^{64}Cu-NOTA-PEG_4-SAA_4-c(RGDfK) (Rt = 17.9 min) were purified by radio-HPLC using a biocompatible water-ethanol mobile phase (Online Resource Fig. S1). Excellent yields (>90%), as per determined by radio-HPLC, and specific activities well above 15 MBq/nmol were obtained. For *in vivo* studies, we diluted the purified fractions with PBS for a final ethanol concentration below 10%.

The hydrophilicity of the three ^{64}Cu-labeled compounds was determined with an octanol-water partition assay. The recorded logP values for ^{64}Cu-NOTA-PEG_4-SAA_4-c(RGDfK), ^{64}Cu-NOTA-$(PEG)_2$-c(RGDfK), and ^{64}Cu-NOTA-c(RGDfK) were −3.40 ± 0.05, −2.82 ± 0.06, and −2.65 ± 0.01, respectively (n = 3).

Competitive cell binding

We investigated and compared the integrin $\alpha_v\beta_3$–binding affinities of c(RGDfK), NOTA-c(RGDfK), NOTA-$(PEG)_2$-c(RGDfK), and NOTA-PEG_4-SAA_4-c(RGDfK) via a competitive binding assay using ^{125}I-echistatin as radio-ligand in U87MG cells (Fig. 2). Upon incubation with increasing concentration of the peptides, we observed a decrease on the U87MG-bound radioactivity indicative of the displacement of the radio-ligand (Fig. 2). Similar IC_{50} values of 254 ± 48, 507 ± 62, 444 ± 41, and 288 ± 66 nM were recorded for c(RGDfK), NOTA-c(RGDfK), NOTA-$(PEG)_2$-c(RGDfK), and NOTA-PEG_4-SAA_4-c(RGDfK), respectively. These results indicate that neither the structural modification of the peptide nor the conjugation of NOTA had a significant impact on the binding affinities of the peptides.

Dynamic PET

Dynamic PET studies were performed to determine and compare the effects of the each structural modification on the early PK properties of the peptides. Mice bearing integrin-positive U87MG tumors were injected with either of the ^{64}Cu-labeled peptides and the temporal *in vivo* biodistribution of the tracer was recorded and quantified. An ROI analysis of the dynamic PET images was performed to determine the time-activity curves of the blood pool, liver, kidneys, muscle, and U87MG tumor (Fig. 3). Given the high correlation between blood tracer concentrations determined by invasive arterial blood sampling and by PET images of the heart's left ventricle [16], we employed an image-based approach to calculate the circulation PK of the tracers. An analysis of the left ventricular activity curves exposed a similar, rapid, clearance of the peptides from the blood circulation. We then calculated the circulation half-life of each tracer via a bi-exponential fitting of the data revealing longer half-lives for ^{64}Cu-NOTA-$(PEG)_2$-c(RGDfK) (4.76 min) and ^{64}Cu-NOTA-PEG_4-SAA_4-c(RGDfK) (4.07 min), compared to ^{64}Cu-NOTA-c(RGDfK) (2.56 min). Liver curves displayed comparable trend for all three peptides, however the absolute %ID/g values of ^{64}Cu-NOTA-c(RGDfK) were the highest in this organ. Kidneys' time-activity curves confirmed renal clearance as the main excretory pathways of the peptides; however, uptake in the kidneys showed a marked difference between ^{64}Cu-NOTA-$(PEG)_2$-c(RGDfK) and the rest of the peptides. Consistently with its longer circulation half-life, ^{64}Cu-NOTA-$(PEG)_2$-c(RGDfK) presented a slower kidney clearance which resulted in prolonged higher accumulation of the tracer in this organ.

The U87MG tumor accretion of the three peptides peaked at comparable values (~4 %ID/g), approximately 10 min after injection; however, ^{64}Cu-NOTA-c(RGDfK)-PEG$_4$-SAA$_4$ exhibited a faster reduction on the magnitude of the uptake, indicative of its faster clearance/degradation. Similarly, the radioactivity in the muscle showed a rapid decline, especially for ^{64}Cu-NOTA-c(RGDfK)-PEG$_4$-SAA$_4$ where uptakes values were found to be the lowest. Nonetheless, better tumor/muscle ratios (Fig 3f) were noted for ^{64}Cu-NOTA-PEG$_4$-SAA$_4$-c(RGDfK), reaching values over 16, 30 min after its administration.

Static PET

Longitudinal static PET scans (n = 3), acquired at 0.5 h, 2 h, and 4 h after the iv injection of ^{64}Cu-NOTA-c(RGDfK), ^{64}Cu-NOTA-(PEG)$_2$-c(RGDfK) or ^{64}Cu-NOTA-PEG$_4$-SAA$_4$-c(RGDfK), were performed to evaluate and compare the “long term” tumor homing and imaging properties of each peptide. PET images of coronal planes intersecting the tumor (Fig 4a) revealed a sharp delineation of the tumor contours in all groups, owing to the attained elevated tumor-to-background ratios (Fig 4b). The results of ROI quantitative analysis of the tracer uptake in blood pool, liver, kidneys, muscle, and U87MG tumors are summarized in Online Resource (Table S1). Compared to the other two peptides, a significantly lower ($P < 0.05$) tumor accumulation of ^{64}Cu-NOTA-PEG$_4$-SAA$_4$-c(RGDfK) (2.50 ± 0.18, 1.77 ± 0.38, 1.67 ± 0.38 %ID/g at 0.5, 2, and 4 h p.i., respectively; n = 3) was observed at all time-points. A similar trend was noted in non-target tissues such as muscle and blood, where ^{64}Cu-NOTA-PEG$_4$-SAA$_4$-c(RGDfK) also displayed significantly lower uptakes, resulting in comparable ($P > 0.05$) contrast ratios. Concurrently with its higher hydrophobicity, the non-specific accretion of ^{64}Cu-NOTA-c(RGDfK) in the liver, muscle, and blood was considerably higher throughout the study. Overall, ^{64}Cu-NOTA-PEG$_4$-SAA$_4$-c(RGDfK) exhibited excellent properties for the imaging of integrin $\alpha_v\beta_3$ that include a faster accumulation in tumor tissue, and a lower overall uptake on non-target organs without compromising the tumor-to-background ratios.

Furthermore, we demonstrated the specific character of the *in vivo* integrin $\alpha_v\beta_3$-binding of ^{64}Cu-NOTA-PEG$_4$-SAA$_4$-c(RGDfK)through a receptor blocking experiment. In this study, mice were administered a larger dose (10 mg/kg) of c(RGDyK)) co-injected with the tracer, and sequential PET scan were acquired. As clearly noticeable in the PET images (Fig. 4a bottom right panel), the co-injection of c(RGDyK) provoked the drastic reduction ($P < 0.01$) on ^{64}Cu-NOTA-PEG$_4$-SAA$_4$-c(RGDfK) tumor uptake values to 0.42 ± 0.14, 0.24 ± 0.06, 0.18 ± 0.03 %ID/g at 0.5, 2, and 4 h p.i., respectively (n = 4; Fig 4b and Online Resource Table S1). An overall reduction in the uptake of some of the non-target tissues evidenced the faster clearance of the tracer that is typical of this sort of experiments.

Biodistribution

In order to validate the accuracy of the PET data and to provide a more comprehensive biodistribution profile of each peptide, we carried out *ex vivo* biodistribution experiments. Immediately after the last PET scan at 4 h p.i., mice were euthanized and the tracer uptake in the blood pool, U87MG tumors, and other major tissue/organs recorded and reported as %ID/g (Fig 5 and Online Resource Table S2). The U87MG tumors uptake values were 2.98 ± 0.52 %ID/g for ^{64}Cu-NOTA-c(RGDfK), 2.36 ± 0.31 %ID/g for ^{64}Cu-NOTA-(PEG)$_2$-

c(RGDfK), and 1.14 ± 0.26 %ID/g for ^{64}Cu-NOTA-PEG$_4$-SAA$_4$-c(RGDfK), which closely resembled the microPET data. Very low blood pool activities were noted for all three peptides, confirming the rapid clearance of these radiolabeled compounds. Accumulation in non-target tissues was low, typically under 1 %ID/g, except in the organs involved in the systemic clearance of the peptides (kidney, liver, intestine, spleen). Of note was that background/residual uptakes of ^{64}Cu-NOTA-c(RGDfK) were much higher than for its counterparts, which can be explained by its higher hydrophobicity. The tumor blocking effect of the injection of a high dose of c(RGDyK) was evidenced in U87MG tumors by a significant decrease on ^{64}Cu-NOTA-PEG$_4$-SAA$_4$-c(RGDfK) uptake, but not in the kidneys where the uptake was not affected (0.96 ± 0.12 vs. 1.78 ± 1.04 %ID/g, in positive vs. blocking group; Fig. 5b and Online Resource Table S2). Also upon blocking, a clear drop on the uptake in the remaining organs was observed, this effect can be attributed to the presence of basal integrin $\alpha_v\beta_3$ expression level in these organs. Nonetheless, the *in vivo* avidity and specificity of the tracers for integrin $\alpha_v\beta_3$ was ratified.

Stability

Serum and urine stability experiments were performed to determine *in vitro*/*in vivo* degradability of ^{64}Cu-NOTA-(PEG)$_2$-c(RGDfK) and ^{64}Cu-NOTA-PEG$_4$-SAA$_4$-c(RGDfK). Online Resource (Fig. S2) displays representative radio-HPLC chromatograms of the tracers after incubation in complete mouse serum or collection from mice urine, 1 h after administration into animals. Neither peptide showed significant levels of degradation after 1 or 4 h incubation in serum (>95% remained intact). The presence of radioactive metabolites was not observed in the urine samples corresponding to either ^{64}Cu-NOTA-(PEG)$_2$-c(RGDfK) or ^{64}Cu-NOTA-PEG$_4$-SAA$_4$-c(RGDfK), confirming peptides stability *in vivo* over a period of 1 h.

Discussion

A significant volume of work has exposed some of the key factors influencing the pharmacokinetics and pharmacodynamics of RGD-based peptides [17]. Several strategies to improve on aspects such as circulation half-life, binding affinity, and enzymatic stability of these probes have been implemented. For example, it is now known that increasing the hydrophilic character of RGD peptides improves its circulation half-lives, whereas cyclization reduces sensitivity toward enzymatic degradation [18, 19], and that multimerization significantly increases the integrin $\alpha_v\beta_3$ binding affinity of these antagonists due to a polyvalence effect [20, 21]. A clear tendency towards focusing on increasing the absolute tumor uptake of RGD-based tracers, through the synthesis of dimeric, trimeric, tetrameric, and even octameric versions of the cyclic RGD can be identified in recent literature [22–27]. However, these strategies result in an increased non-specific uptake of the peptides on off-target tissues. For example, RGD multimers show significant accumulation on the liver and gut [28], which limits the applicability of these tracers to detect tumors located in the abdominal cavity. Additionally, the claimed polyvalence effect would require elevated levels of integrin $\alpha_v\beta_3$ expression within the tumor in order to provide a significant targeting advantage over monomers [29]. In this study, we sought to revisit the imaging of integrin $\alpha_v\beta_3$ using monomeric c(RGDfK) peptides with enhanced imaging properties.

Several studies demonstrated that the alteration of RGD peptides using polyethylene glycol and/or galactose linkers positively influence its PK/PD properties [17, 20, 21, 28–31]. Based on that precedent, we developed two peptides $(PEG)_2$-c(RGDfK) and PEG_4-SAA_4-c(RGDfK) through the derivatization of a c(RGDfK) monomer with the hydrophilic linkers PEG and PEG_4-SAA_4.

The two derivatives and the unmodified c(RGDfK) were conjugated to NOTA for the posterior ^{64}Cu-labeling and PET imaging. The lower logP (-3.40 ± 0.05) value and shorter retention time of ^{64}Cu-NOTA-PEG_4-SAA_4-c(RGDfK) (R_t = 17.9 min) in C18 chromatographic columns evidenced a marked hydrophilic character compared to the other tracers. The integrin $\alpha_v\beta_3$ binding properties of the NOTA-conjugated peptides were compared to the unmodified c(RGDfK) through an *in vitro* cell binding assay, which revealed binding affinities in the nM range for all compounds. The highest receptor affinity, which was close to that of the c(RGDfK) peptide (254 ± 48 nM), was observed for NOTA-PEG_4-SAA_4-c(RGDfK) (288 ± 66 nM) presumably due to its higher conformational freedom and improved hydrophilicity.

Both radiolabeled tracers, ^{64}Cu-NOTA-$(PEG)_2$-c(RGDfK) and ^{64}Cu-NOTA-PEG_4-SAA_4-c(RGDfK) displayed a reduced *in vivo* accumulation in non-target tissues including intestines, liver, kidneys, and muscle compared to the native ^{64}Cu-NOTA-c(RGDfK) peptide. The pharmacokinetic advantage of the modified peptides in terms of background distribution was expected and justified given their higher molecular weight and hydrophilic character, which was evidenced by their clear tendency to remain within the blood pool compartment (both showed slightly longer blood circulation half-lives). For the same reasons, uptake of the derivatized peptides was lower in the U87MG tumors: 3.62 ± 0.21 %ID/g and 2.76 ± 0.04 %ID/g vs. 4.78 ± 0.74 %ID/g at 30 min p.i. for ^{64}Cu-NOTA-$(PEG)_2$-c(RGDfK), ^{64}Cu-NOTA-PEG_4-SAA_4-c(RGDfK) and ^{64}Cu-NOTA-c(RGDfK), respectively. However, the observed tumor/muscle, tumor/blood, tumor/liver, and tumor/kidney contrast ratios (Online Resource Tables S3 and S4) were either superior or remained comparable to those of ^{64}Cu-NOTA-c(RGDfK) at 30 min, 2 h, and 4 h after injection of the imaging peptides. Other ^{64}Cu-labelled monomeric RGD peptides have been reported showing similar tumor-to-normal tissue ratios [32], but in those cases imaging at delayed time points was required to attain such high contrast ratios. Altogether, these findings demonstrated the benefits of the addition of the PEG and PEG_4-SAA_4 linkers for the improvement of the imaging properties of c(RGDfK) peptides.

When compared, ^{64}Cu-NOTA-$(PEG)_2$-c(RGDfK) and ^{64}Cu-NOTA-PEG_4-SAA_4-c(RGDfK) ability to target integrin $\alpha_v\beta_3$ *in vivo* seemed to contradict the results of the *in vitro* binding affinity studies. In spite of its higher integrin $\alpha_v\beta_3$-binding affinity, ^{64}Cu-NOTA-PEG_4-SAA_4-c(RGDfK) displayed lower *in vivo* accretion in the U87MG tumor xenografts. Once more, it is likely that hydrophilicity played a central role in enhancing the overall excretion of the tracer form the mouse body, which resulted in a reduced bio-availability of the compound. Nonetheless, ^{64}Cu-NOTA-PEG_4-SAA_4-c(RGDfK) provided a faster, superior tumor/muscle contrast (16.6 ± 5.6; Fig. 3f) within half hour after administration of the radiolabeled peptide. Renal excretion was the main excretory pathway for both compounds; however, the analysis of kidney's time-activity curves (Fig. 3c) unveiled a lower

integral ^{64}Cu-NOTA-PEG$_4$-SAA$_4$-c(RGDfK) kidney uptake. This translates into lower procedural radiation doses and in a reduction on the chances of development renal radiotoxicity upon repeated imaging (kidneys are common dose-limiting organs for peptide-based radiopharmaceuticals). Furthermore, the specificity of ^{64}Cu-NOTA-PEG$_4$-SAA$_4$-c(RGDfK) tumor uptake was confirmed via a receptor blocking study where the co-injection of an c(RGDyK) excess (10 mg/kg) decreased tumor uptake to ~10% of the unblocked %ID/g value. Several non-target tissues (liver, lung, spleen, kidney, and intestine) also experienced a partial blocking effect, consistently with the basal integrin $\alpha_v\beta_3$ expression levels reported for these tissues in both rodents and humans [33–35].

Over the last decade, the study of the integrin $\alpha_v\beta_3$ expression, as a sensitive indicator of tumor angiogenesis, using RGD peptides has shown great success [9, 36]. Without doubt, nuclear diagnostic imaging, which has become an indispensable tool for the exploration of tumor biology in a clinical setting, has been one of the areas where RGD's potentiality has been vastly exploited. A myriad of RGD-based radiotracer for PET imaging have emerged, resulting on the clinical evaluation of several [12, 13, 37–39]; however, these studies demonstrates that significant improvements are still required for a successful clinical implementation. An ideal molecular imaging radiotracer should able to accumulate rapidly and specifically within the target tissue to provide a high target-to-background contrast, while quickly excreting from the rest of the body, minimizing radiation burden and permitting the repeated imaging with little adverse effects[40]. Additionally, it should be easy to synthesize and must feature a radionuclide with properties (decay mode, energy, $t_{1/2}$, etc.) that allows its rapid and sensitive detection within a short period after administration. Hence, our results strongly indicate that ^{64}Cu-NOTA-PEG$_4$-SAA$_4$-c(RGDfK) possesses the necessary traits to be considered as an excellent radiotracer to provide fast, specific, and high-contrast imaging of integrin $\alpha_v\beta_3$ expression with potentially minimal adverse effects. Moreover, its fast kinetics facilitates the implementation of analogous radiotracers using isotopes with a short half-life such as ^{18}F and ^{68}Ga.

In conclusion, we presented the facile radiosynthesis and evaluation of two novel RGD-based radiotracers with enhanced PK properties for the noninvasive imaging of tumor associated integrin $\alpha_v\beta_3$ using PET. The synthesized compounds displayed strong and specific integrin $\alpha_v\beta_3$-binding, and very high metabolic stability both *in vitro* and *in vivo*. Both tracers showed an enhanced overall clearance resulting in lower uptake in background tissues including kidneys, lungs, liver, intestine, and spleen. These results demonstrated the benefits of the PEG and PEG$_4$-SAA$_4$ derivatization of RDG peptides for high-contrast noninvasive PET imaging of integrin $\alpha_v\beta_3$ expression, especially in abdominally located malignancies where high off-target uptakes make detection difficult.

Supplementary Material

Refer to Web version on PubMed Central for supplementary material.

Acknowledgments

Funding: This study was funded by the University of Wisconsin–Madison, the Department of Defense (W81XWH-11-1-0644 & W81XWH-11-1-0648), the National Science Foundation (DGE-1256259), the National

Institutes of Health (NIBIB/NCI 1R01CA169365, P30CA014520, T32CA009206, and 5T32GM08349), the US Department of States sponsored Fulbright Scholar Program (1831/FNPDR/2013), and the American Cancer Society (125246-RSG-13-099-01-CCE).

References

1. Hwang R, Varner J. The role of integrins in tumor angiogenesis. Hematol Oncol Clin North Am. 2004; 18:991–1006. vii. [PubMed: 15474331]
2. Robinson SD, Hodivala-Dilke KM. The role of beta3-integrins in tumor angiogenesis: context is everything. Curr Opin Cell Biol. 2011; 23:630–7. [PubMed: 21565482]
3. Puduvalli VK. Inhibition of angiogenesis as a therapeutic strategy against brain tumors. Cancer Treat Res. 2004; 117:307–36. [PubMed: 15015567]
4. Sengupta S, Chattopadhyay N, Mitra A, Ray S, Dasgupta S, Chatterjee A. Role of alphavbeta3 integrin receptors in breast tumor. J Exp Clin Cancer Res. 2001; 20:585–90. [PubMed: 11876555]
5. Felding-Habermann B, Fransvea E, O'Toole TE, Manzuk L, Faha B, Hensler M. Involvement of tumor cell integrin alpha v beta 3 in hematogenous metastasis of human melanoma cells. Clin Exp Metastasis. 2002; 19:427–36. [PubMed: 12198771]
6. Jin H, Varner J. Integrins: roles in cancer development and as treatment targets. Br J Cancer. 2004; 90:561–5. [PubMed: 14760364]
7. Kumar CC. Integrin alpha v beta 3 as a therapeutic target for blocking tumor-induced angiogenesis. Curr Drug Targets. 2003; 4:123–31. [PubMed: 12558065]
8. Kumar CC, Armstrong L, Yin Z, Malkowski M, Maxwell E, Ling H, et al. Targeting integrins alpha v beta 3 and alpha v beta 5 for blocking tumor-induced angiogenesis. Adv Exp Med Biol. 2000; 476:169–80. [PubMed: 10949664]
9. Cai W, Niu G, Chen X. Imaging of integrins as biomarkers for tumor angiogenesis. Curr Pharm Des. 2008; 14:2943–73. [PubMed: 18991712]
10. Schottelius M, Laufer B, Kessler H, Wester HJ. Ligands for mapping alphavbeta3-integrin expression in vivo. Acc Chem Res. 2009; 42:969–80. [PubMed: 19489579]
11. Gaertner FC, Kessler H, Wester HJ, Schwaiger M, Beer AJ. Radiolabelled RGD peptides for imaging and therapy. Eur J Nucl Med Mol Imaging. 2012; 39 (Suppl 1):S126–38. [PubMed: 22388629]
12. Kenny LM, Coombes RC, Oulie I, Contractor KB, Miller M, Spinks TJ, et al. Phase I trial of the positron-emitting Arg-Gly-Asp (RGD) peptide radioligand 18F-AH111585 in breast cancer patients. J Nucl Med. 2008; 49:879–86. [PubMed: 18483090]
13. Beer AJ, Haubner R, Sarbia M, Goebel M, Luderschmidt S, Grosu AL, et al. Positron emission tomography using [18F]Galacto-RGD identifies the level of integrin alpha(v)beta3 expression in man. Clin Cancer Res. 2006; 12:3942–9. [PubMed: 16818691]
14. Jeong JM, Hong MK, Chang YS, Lee YS, Kim YJ, Cheon GJ, et al. Preparation of a promising angiogenesis PET imaging agent: 68Ga-labeled c(RGDyK)-isothiocyanatobenzyl-1,4,7-triazacyclononane-1,4,7-triacetic acid and feasibility studies in mice. J Nucl Med. 2008; 49:830–6. [PubMed: 18413379]
15. Hernandez R, Valdovinos HF, Yang Y, Chakravarty R, Hong H, Barnhart TE, et al. (44)Sc: An Attractive Isotope for Peptide-Based PET Imaging. Mol Pharm. 2014; 11:2954–61. [PubMed: 25054618]
16. Kim SJ, Lee JS, Im KC, Kim SY, Park SA, Lee SJ, et al. Kinetic modeling of 3′-deoxy-3′-18F-fluorothymidine for quantitative cell proliferation imaging in subcutaneous tumor models in mice. J Nucl Med. 2008; 49:2057–66. [PubMed: 18997037]
17. Haubner R, Decristoforo C. Radiolabelled RGD peptides and peptidomimetics for tumour targeting. Front Biosci (Landmark Ed). 2009; 14:872–86. [PubMed: 19273105]
18. Bogdanowich-Knipp SJ, Chakrabarti S, Williams TD, Dillman RK, Siahaan TJ. Solution stability of linear vs. cyclic RGD peptides. J Pept Res. 1999; 53:530–41. [PubMed: 10424348]
19. Samanen J, Ali F, Romoff T, Calvo R, Sorenson E, Vasko J, et al. Development of a small RGD peptide fibrinogen receptor antagonist with potent antiaggregatory activity in vitro. J Med Chem. 1991; 34:3114–25. [PubMed: 1920361]

20. Haubner R, Wester HJ, Burkhart F, Senekowitsch-Schmidtke R, Weber W, Goodman SL, et al. Glycosylated RGD-containing peptides: tracer for tumor targeting and angiogenesis imaging with improved biokinetics. J Nucl Med. 2001; 42:326–36. [PubMed: 11216533]
21. Haubner R, Wester HJ, Weber WA, Mang C, Ziegler SI, Goodman SL, et al. Noninvasive imaging of alpha(v)beta3 integrin expression using 18F-labeled RGD-containing glycopeptide and positron emission tomography. Cancer Res. 2001; 61:1781–5. [PubMed: 11280722]
22. Li ZB, Cai W, Cao Q, Chen K, Wu Z, He L, et al. (64)Cu-labeled tetrameric and octameric RGD peptides for small-animal PET of tumor alpha(v)beta(3) integrin expression. J Nucl Med. 2007; 48:1162–71. [PubMed: 17574975]
23. Liu S. Radiolabeled multimeric cyclic RGD peptides as integrin alphavbeta3 targeted radiotracers for tumor imaging. Mol Pharm. 2006; 3:472–87. [PubMed: 17009846]
24. Auzzas L, Zanardi F, Battistini L, Burreddu P, Carta P, Rassu G, et al. Targeting alphavbeta3 integrin: design and applications of mono-and multifunctional RGD-based peptides and semipeptides. Curr Med Chem. 2010; 17:1255–99. [PubMed: 20166941]
25. Dijkgraaf I, Yim CB, Franssen GM, Schuit RC, Luurtsema G, Liu S, et al. PET imaging of alphavbeta(3) integrin expression in tumours with (6)(8)Ga-labelled mono-, di-and tetrameric RGD peptides. Eur J Nucl Med Mol Imaging. 2011; 38:128–37. [PubMed: 20857099]
26. Notni J, Pohle K, Wester HJ. Be spoilt for choice with radiolabelled RGD peptides: preclinical evaluation of (6)(8)Ga-TRAP(RGD)(3). Nucl Med Biol. 2013; 40:33–41. [PubMed: 22995902]
27. Knetsch PA, Zhai C, Rangger C, Blatzer M, Haas H, Kaeopookum P, et al. [(68)Ga]FSC-(RGD)3 a trimeric RGD peptide for imaging alphavbeta3 integrin expression based on a novel siderophore derived chelating scaffold-synthesis and evaluation. Nucl Med Biol. 2015; 42:115–22. [PubMed: 25459110]
28. Shi J, Kim YS, Zhai S, Liu Z, Chen X, Liu S. Improving tumor uptake and pharmacokinetics of (64)Cu-labeled cyclic RGD peptide dimers with Gly(3) and PEG(4) linkers. Bioconjug Chem. 2009; 20:750–9. [PubMed: 19320477]
29. Ji S, Czerwinski A, Zhou Y, Shao G, Valenzuela F, Sowinski P, et al. (99m)Tc-Galacto-RGD2: a novel 99mTc-labeled cyclic RGD peptide dimer useful for tumor imaging. Mol Pharm. 2013; 10:3304–14. [PubMed: 23875883]
30. Liu S, Liu Z, Chen K, Yan Y, Watzlowik P, Wester HJ, et al. 18F-labeled galacto and PEGylated RGD dimers for PET imaging of alphavbeta3 integrin expression. Mol Imaging Biol. 2010; 12:530–8. [PubMed: 19949981]
31. Jung KH, Lee KH, Paik JY, Ko BH, Bae JS, Lee BC, et al. Favorable biokinetic and tumor-targeting properties of 99mTc-labeled glucosamino RGD and effect of paclitaxel therapy. J Nucl Med. 2006; 47:2000–7. [PubMed: 17138743]
32. Dumont RA, Deininger F, Haubner R, Maecke HR, Weber WA, Fani M. Novel (64)Cu- and (68)Ga-labeled RGD conjugates show improved PET imaging of alpha(nu)beta(3) integrin expression and facile radiosynthesis. J Nucl Med. 2011; 52:1276–84. [PubMed: 21764795]
33. Zhang X, Xiong Z, Wu Y, Cai W, Tseng JR, Gambhir SS, et al. Quantitative PET imaging of tumor integrin alphavbeta3 expression with 18F-FRGD2. J Nucl Med. 2006; 47:113–21. [PubMed: 16391195]
34. Wu Z, Li ZB, Chen K, Cai W, He L, Chin FT, et al. microPET of tumor integrin alphavbeta3 expression using 18F-labeled PEGylated tetrameric RGD peptide (18F-FPRGD4). J Nucl Med. 2007; 48:1536–44. [PubMed: 17704249]
35. Behr TM, Goldenberg DM, Becker W. Reducing the renal uptake of radiolabeled antibody fragments and peptides for diagnosis and therapy: present status, future prospects and limitations. Eur J Nucl Med. 1998; 25:201–12. [PubMed: 9473271]
36. Cai W, Chen X. Multimodality molecular imaging of tumor angiogenesis. J Nucl Med. 2008; 49 (Suppl 2):113S–28S. [PubMed: 18523069]
37. Doss M, Kolb HC, Zhang JJ, Belanger MJ, Stubbs JB, Stabin MG, et al. Biodistribution and radiation dosimetry of the integrin marker 18F-RGD-K5 determined from whole-body PET/CT in monkeys and humans. J Nucl Med. 2012; 53:787–95. [PubMed: 22499613]

38. Wan W, Guo N, Pan D, Yu C, Weng Y, Luo S, et al. First experience of 18F-alfatide in lung cancer patients using a new lyophilized kit for rapid radiofluorination. J Nucl Med. 2013; 54:691–8. [PubMed: 23554506]

39. Liu Z, Wang F. Development of RGD-based radiotracers for tumor imaging and therapy: translating from bench to bedside. Curr Mol Med. 2013; 13:1487–505. [PubMed: 24206140]

40. Torchilin, VP. Handbook of targeted delivery of imaging agents. Torchilin, VP., editor. CRC Press; 1995.

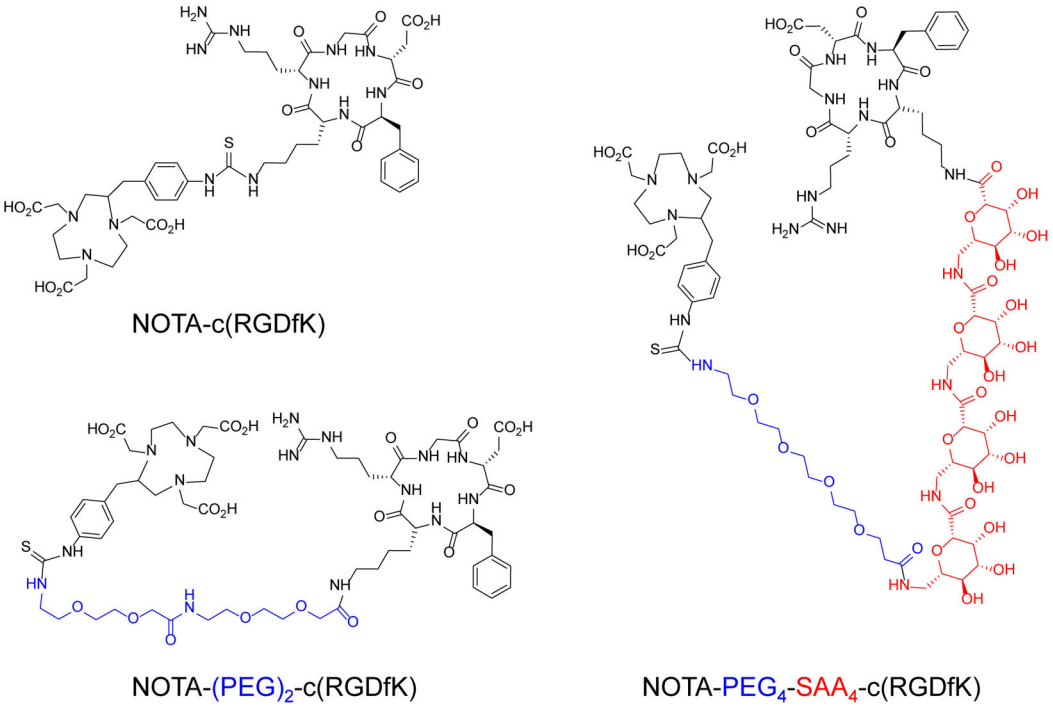

Fig. 1.

Chemical structures of NOTA-c(RGDfK), NOTA-$(PEG)_2$-c(RGDfK), and NOTA-PEG_4-SAA_4-c(RGDfK)

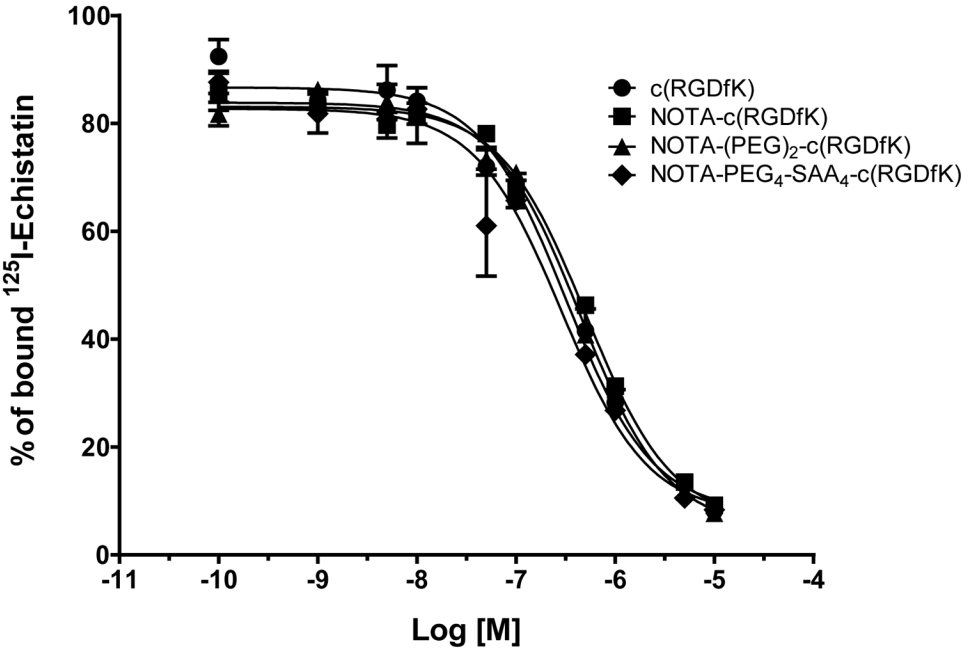

Fig. 2.

Concentration dependent inhibition of ^{125}I-echistatin binding to integrin $\alpha_v\beta_3$ in U87MG cells by c(RGDfK), NOTA-c(RGDfK), NOTA-$(PEG)_2$-c(RGDfK), or NOTA-PEG_4-SAA_4-c(RGDfK). Solid circles: c(RGDfK) (IC_{50} = 254 ± 48 nM); solid squares: NOTA-c(RGDfK) (IC_{50} = 507 ± 62 nM); solid triangles: NOTA-$(PEG)_2$-c(RGDfK) (IC_{50} = 444 ± 41 nM); solid rhomboids: NOTA-PEG_4-SAA_4-c(RGDfK) (IC_{50} = 288 ± 66 nM)

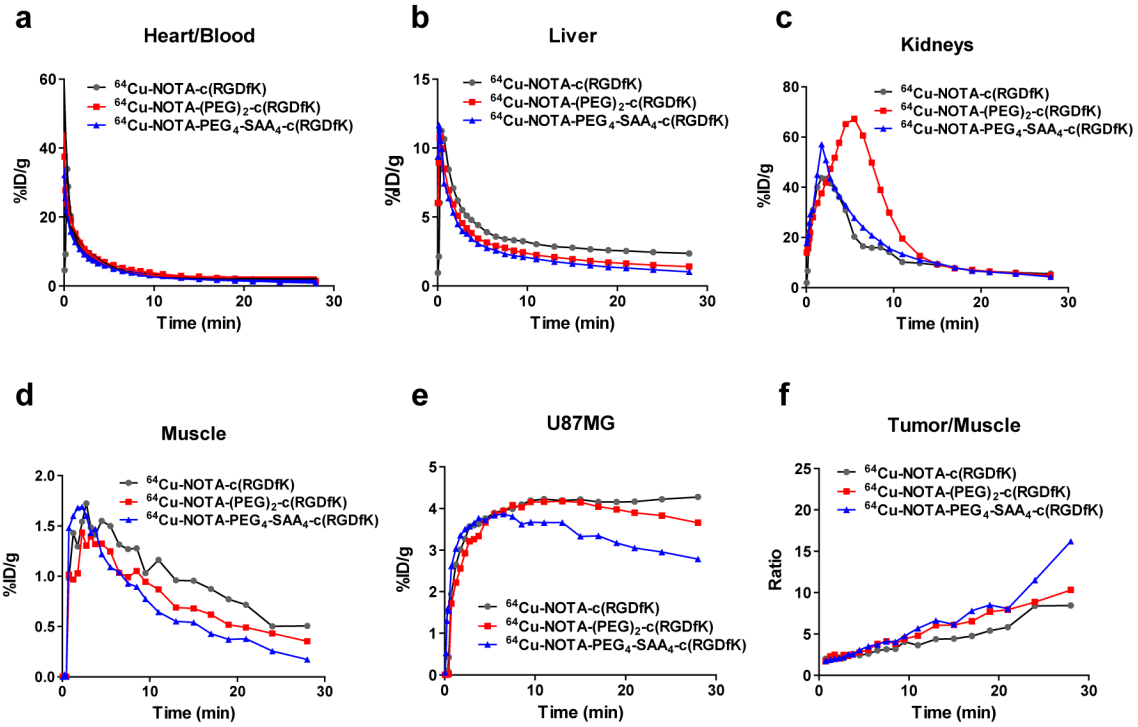

Fig. 3.

Dynamic PET-derived time-activity distribution of ^{64}Cu-NOTA-c(RGDfK), ^{64}Cu-NOTA-(PEG)$_2$-c(RGDfK), or ^{64}Cu-NOTA-PEG$_4$-SAA$_4$-c(RGDfK) in blood pool (a), liver (b), kidneys (c), muscle (d), and tumor (e) in nude mice bearing U87MG xenografts, during the first 30 min after injection of 5.5 MBq of the tracers. (f) Time progression of the early tumor-to-muscle ratios for each of the radiolabeled peptides.

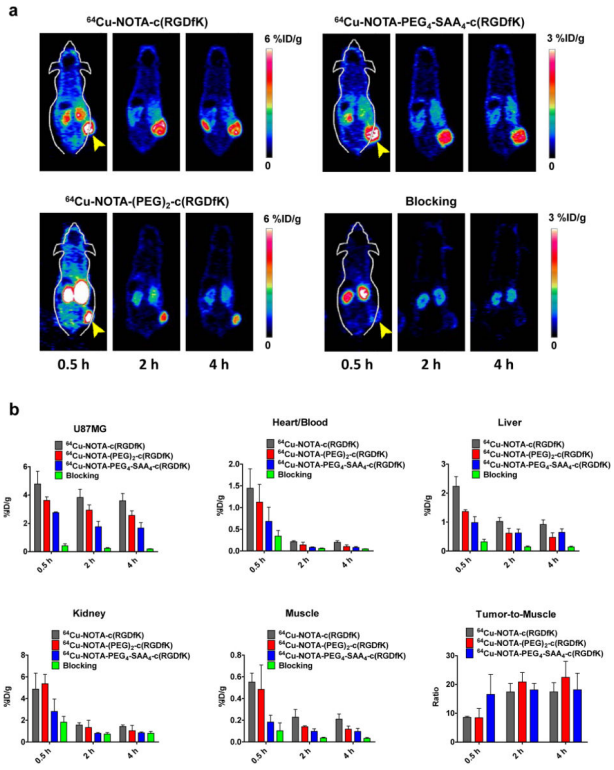

Fig. 4.

Noninvasive microPET imaging of tumor-associated integrin $\alpha_v\beta_3$ in athymic nude mice bearing U87MG tumors. (a) Representative coronal PET images of planes containing U87MG tumors, at 30 min, 2, and 4 h after intravenous injection of 5.5 MBq of ^{64}Cu-NOTA-c(RGDfK), ^{64}Cu-NOTA-$(PEG)_2$-c(RGDfK), ^{64}Cu-NOTA-PEG_4-SAA_4-c(RGDfK), or ^{64}Cu-NOTA-PEG_4-SAA_4-c(RGDfK) coinjected with an c(RGDyK) (10mg/kg) blocking dose; yellow arrow heads indicate the location of the tumor. (b) Quantitative analysis of the PET images showing the timecourse of the accumulation of the tracers in U87MG tumor, blood pool, liver, kidneys, and muscle. Uptake values are expressed as %ID/g ± SD (n = 3). Bottom right panel describes the tumor-to-muscle ratios attained with each of the radiolabeled peptides.

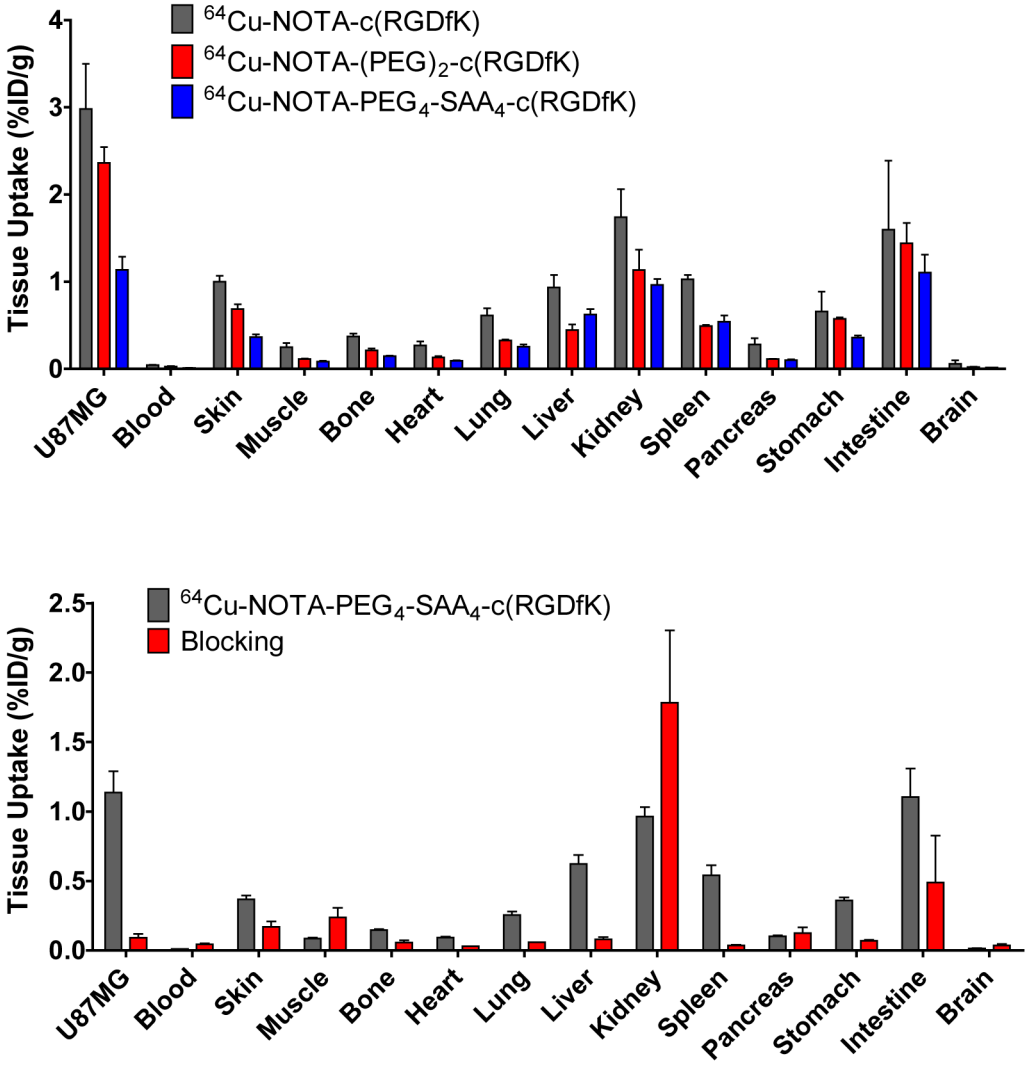

Fig. 5.

(a) *Ex vivo* biodistribution data of ^{64}Cu-NOTA-c(RGDfK), ^{64}Cu-NOTA-$(PEG)_2$-c(RGDfK), and ^{64}Cu-NOTA-PEG_4-SAA_4-c(RGDfK) in U87MG bearing nude mice, 4 h after injection. (b) Comparison of the 4 h p.i. biodistribution profile ^{64}Cu-NOTA-PEG_4-SAA_4-c(RGDfK) with and without the coinjection of an c(RGDyK) (10mg/kg) blocking dose. Data are represented as %ID/g ± SD (n=3).